

Article

Impact of ZnO Modifier Concentration on TeO₂ Glass Matrix for Optical and Gamma-Ray Shielding Capabilities

Dalal A. Aloraini ¹, M. I. Sayyed ^{2,*} , Ashok Kumar ^{3,4}, Sabina Yasmin ⁵  and Aljawhara H. Almuqrin ¹

¹ Department of Physics, College of Science, Princess Nourah Bint Abdulrahman University, P.O. Box 84428, Riyadh 11671, Saudi Arabia; daalorainy@pnu.edu.sa (D.A.A.); ahalmoqren@pnu.edu.sa (A.H.A.)

² Department of Physics, Faculty of Science, Isra University, Amman 11622, Jordan

³ Department of Physics, University College Benra, Dhuri 148024, Punjab, India; ajindal9999@gmail.com

⁴ Department of Physics, Punjabi University, Patiala 147002, Punjab, India

⁵ Department of Physics, Chittagong University of Engineering and Technology, Chattogram 4349, Bangladesh; sabinayasmin309@gmail.com

* Correspondence: dr.mabualssayed@gmail.com

Abstract: This study carried out a comparison of the optical and gamma ray shielding features of TeO₂ with and without ZnO modifier concentration. Incorporating ZnO into the TeO₂ network reduces the indirect band gap from 3.515–3.481 eV. When ZnO is added, refractive indices, dielectric constants, and optical dielectric constants rise from 2.271–2.278, 5.156–5.191, and 4.156–4.191 accordingly. The transmission coefficient and reflection loss are in direct opposition to each other. With increasing ZnO concentration in the selected glasses, the values of molar refractivity and molar polarizability decrease from 18.767–15.018 cm³/mol and from 7.444×10^{-24} – 5.957×10^{-24} cm³, respectively, while the electronic polarizability rises from 8.244×10^{24} – 8.273×10^{24} , correspondingly. As expected by the metallization values, the glass systems are non-metallic. The linear attenuation coefficients (LAC) of the studied glass samples ensue through enhancing the photon energy range 0.0395–0.3443 MeV. There is a very slow decrease in the LAC from an energy of 0.1218–0.3443 MeV, yet there is a sharp decrease from an energy of 0.0401–0.0459 MeV. According to the obtained values of numerous shielding parameters such as LAC, MAC, HVL, MFP, and Z_{eff} sample, Zn30 has shown the best radiation shielding ability comprising other studied samples.

Keywords: optical dielectric constant; ZnO; transmission coefficient; low energy



Citation: Aloraini, D.A.; Sayyed, M.I.; Kumar, A.; Yasmin, S.; Almuqrin, A.H. Impact of ZnO Modifier Concentration on TeO₂ Glass Matrix for Optical and Gamma-Ray Shielding Capabilities. *Materials* **2022**, *15*, 5342. <https://doi.org/10.3390/ma15155342>

Academic Editor: It-Meng (Jim) Low

Received: 29 June 2022

Accepted: 29 July 2022

Published: 3 August 2022

Publisher's Note: MDPI stays neutral with regard to jurisdictional claims in published maps and institutional affiliations.



Copyright: © 2022 by the authors. Licensee MDPI, Basel, Switzerland. This article is an open access article distributed under the terms and conditions of the Creative Commons Attribution (CC BY) license (<https://creativecommons.org/licenses/by/4.0/>).

1. Introduction

With the remarkable development in radiation technology, researchers' attention has been focused on radiation shielding materials. These materials are utilized for a variety of industrial and radiologic applications. They are frequently used to attenuate the intensity of the radiations and thus help in protecting the workers, patients, and people from the ionizing radiation. Lead is one of the first materials utilized to manufacture radiation shielding materials [1–4]. The high density of lead has made it a promising shielding material until now. The intensive studies carried out in the radiation shielding materials field have found that lead has some disadvantages, and for this reason, radiation shielding material technologists have produced alternative free lead radiation shielding materials [5–10]. Among these novel materials, glasses have many advantages and possess unique features that encourage those interested in this field to develop novel glass systems in different shielding applications [11–13]. These unique features include the simplicity in synthesis of the glasses with low cost, the good mechanical properties of the glasses, the high transparency, and the high density of the glasses in comparison with other materials such as polymer, concrete, and bricks [14,15]. These outstanding features make the glasses ideal to be utilized for radiation protection applications. Due to the high possibilities in

various fields, the continuous attempts in new glass systems and the investigation of their radiation attenuation competence are needed. TeO₂-based glasses have received notable attention from radiation shielding developers since they have a low melting point, good mechanical strength, high refractive index, high density, high effective atomic number, low toxicity, and low tenth value layer [16,17]. Aşkın et al. have studied the gamma shielding potential of the newly established glass system through the Geant4 code. At energy ranges 0.284, 0.356, 0.511, 0.662, 1.17, 3, and 1.330 MeV, Tellurite glass containing 25% moles of Ag₂O showed the maximum mass attenuation coefficient and Z_{eff}, however, the lowermost value of transmission fractions. The fast neutron removal cross-section (ΣR) of the studied glasses amplified with the upsurge of Ag₂O fraction as well as the ΣR values were greater than commonly used concrete material but a close value to the NiO and PbO-containing borate glasses [18]. Sharma et al. investigated zinc tellurite glasses doped with Nd₂O₃. Having the greatest percentage of Nd₂O₃ (0.05) presented a larger shielding capability to some commercial glasses [19]. Bektasoglua et al. investigated the mass attenuation coefficients of the ZnO–TeO₂–Nb₂O₅–Gd₂O₃ glass system at 20, 30, 40, and 60 keV. In the studied samples, the increasing contribution of Gd₂O₃ decreased the value of HVL and increased the value of Z_{eff}. At energy 60 keV, glass samples with 1.5, 2, and 2.5 contributions of Gd₂O₃ showed greater mass attenuation coefficients than lead [20]. Nazrin et al. studied boro-tellurite glasses doped with copper oxide. That studied glass showed an irregular trend with fluctuations within certain limits of elastic moduli [21]. Fidan et al. examined the radiation shielding ability of TeO₂–BaO–B₂O₃–PbO–V₂O₅ glass systems through some shielding parameters. At an energy of 59.5 keV, albedo parameters were also assessed. The intensity of the exposure build-up factor spectra decreased as the mol% of BaO increased. Considering the albedo parameters, BaO represented the maximum reflective compound among the studied glasses [22]. Geidam et al. examined (100 – x) [56TeO₂ – 24B₂O₃ – 20SiO₂] – xBi₂O₃, where x = 0, 1, 2, 3, 4, and 5 mol%, lead-free silica boro-tellurite glasses. With the increase in mol% of Bi₂O₃, the nonlinear variation found for the molar volume and density showed. Studied BSBT5 glass with a higher amount of Bi₂O₃ mol% displayed supreme values of density and linear attenuation coefficient [23]. Ersundu et al. prepared ZnO–MoO₃–TeO₂ glasses. The increase in MoO₃ on the studied glass systems made them stronger as well as amplified mechanical properties. Studied glass systems displayed lower MFP values comprising concretes and window glass [24]. As a continuation of the previous studies in the TeO₂-based glasses as promising radiation shielding materials, we selected binary zinc–tellurite glasses and investigated different radiation shielding parameters for the selected glasses.

2. Materials and Methods

The elemental composition of the studied samples was obtained from Effendy et al. [25]. The samples are coded as Zn0, Zn5, Zn10, Zn15, Zn20, Zn25, and Zn30 respectively:

Zn0: 0 ZnO–100 TeO₂ (density = 4.939 g/cm³)

Zn5: 5 ZnO–95 TeO₂ (density = 4.967 g/cm³)

Zn10: 10 ZnO–90 TeO₂ (density = 4.989 g/cm³)

Zn15: 15 ZnO–85 TeO₂ (density = 5.049 g/cm³)

Zn20: 20 ZnO–80 TeO₂ (density = 5.114 g/cm³)

Zn25: 25 ZnO–75 TeO₂ (density = 5.222 g/cm³)

Zn30: 30 ZnO–70 TeO₂ (density = 5.283 g/cm³)

The optical characteristics of the glasses would be affected by changes in the composition of the glass forming and glass modifiers. The diverse optical fields are predicted to benefit from the combination of ZnO and tellurite glass networks. Table 1 shows the indirect band gap values. With the help of these, we may glean further information about

the optical system. The high concentration of TeO₂ in these glasses is believed to provide them with exceptional radiation shielding capabilities. Using ZnO as a glass modifier, the optical and gamma-ray shielding capabilities of the TeO₂ glassy network were examined in this study. The Phy-X/PSD computer software was utilized for determining the shielding properties of glasses against gamma rays [26]. Our prior reports [27–29] outline the formulas we used to calculate optical and gamma-ray shielding parameters.

Table 1. UV parameters of present glasses.

Properties	Glass Samples						
	Zn0	Zn5	Zn10	Zn15	Zn20	Zn25	Zn30
The indirect band gap (eV)	3.515	3.505	3.499	3.501	3.513	3.504	3.481
n	2.271	2.273	2.274	2.274	2.271	2.273	2.278
ε	5.156	5.166	5.172	5.170	5.158	5.167	5.191
$p \frac{dp}{dt}$	4.156	4.166	4.172	4.170	4.158	4.167	4.191
R _L	0.151	0.151	0.151	0.151	0.151	0.151	0.152
T	0.738	0.737	0.737	0.737	0.738	0.737	0.736
R _m (cm ³ /mol)	18.767	18.223	17.698	17.033	16.352	15.593	15.018
α _m × 10 ^{−24} cm ³	7.444	7.228	7.0203	6.756	6.486	6.185	5.957
α _e × 10 ²⁴	8.244	8.252	8.257	8.256	8.246	8.253	8.273
M	0.151	0.151	0.151	0.151	0.151	0.151	0.152
M (E _g)	0.088	0.088	0.087	0.088	0.088	0.088	0.087
M (n)	0.419	0.419	0.418	0.418	0.419	0.419	0.417
χ ⁽¹⁾	0.331	0.332	0.332	0.332	0.331	0.332	0.334
χ*	0.945	0.942	0.941	0.941	0.944	0.942	0.936
χ ³ × 10 ^{−16} (esu)	2.620	2.602	2.591	2.594	2.616	2.600	2.558
n ₂ ^{optical} × 10 ^{−15} (esu)	4.348	4.313	4.292	4.299	4.341	4.310	4.230

3. Results and Discussion

3.1. Optical Features

A decrease in the indirect band gap value from 3.515 eV to 3.481 eV was observed once ZnO was introduced into the TeO₂ network. The tellurite glass network's regular structure is disrupted by an increase in the network's non-bridging oxygens (NBOs) when ZnO is added. The structure of the glass will become more erratic as the NBO content rises. Indirect optical band gaps are reduced because the NBO electron bonding is less tight than the bonding oxygen, which weakens the glass networks. One possible explanation for a rise in Zn20's optical band gap value is that delocalized states are becoming less common, which reduces the number of trap centers. For the remaining optical properties indicated in Table 1, it utilizes the indirect band gap energy estimates.

The variation in the several optical properties with the numerous concentrations of ZnO on the studied glass samples has been represented in Figures 1–5.

Figure 1 has shown the difference in the refractive index (n), ε and optical dielectric constant considering the amount of ZnO. The n, ε, and optical dielectric constant ($p \frac{dp}{dt}$) values for the increase in NBOs in the network, increase from 2.271–2.278, 5.156–5.191, and 4.156–4.191, respectively, due to the causes of adding ZnO to the samples.

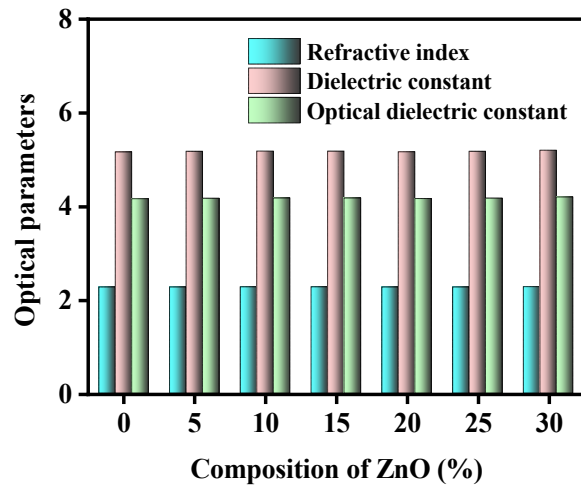


Figure 1. Discrepancy of the refractive index (n), dielectric constant (ϵ), and optical dielectric constant considering the amount of ZnO.

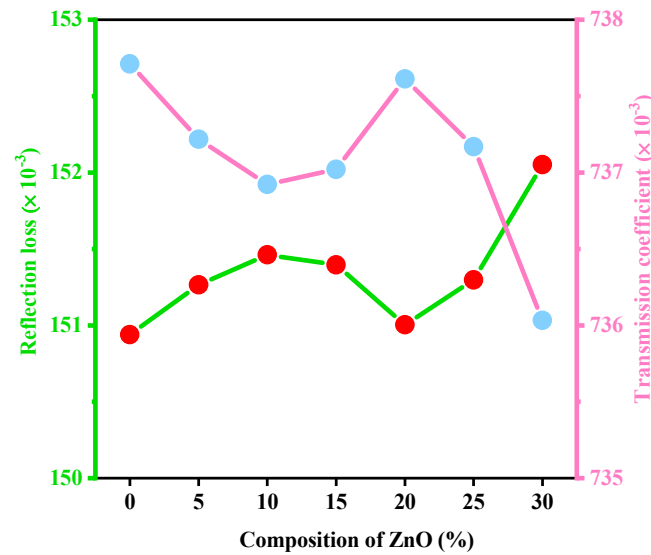


Figure 2. Variation in reflection loss (R_L) and transmission coefficient (T) considering the amount of ZnO.

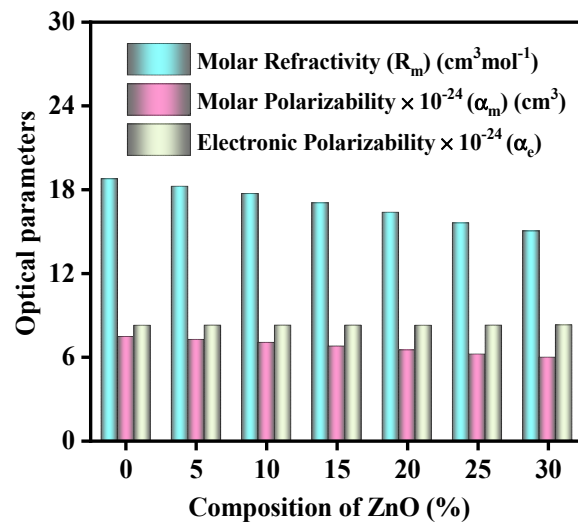


Figure 3. Variation in the molecular polarizability (α_m), the molecular refractivity (R_m), and the electronic polarizability (α_e) considering the amount of ZnO.

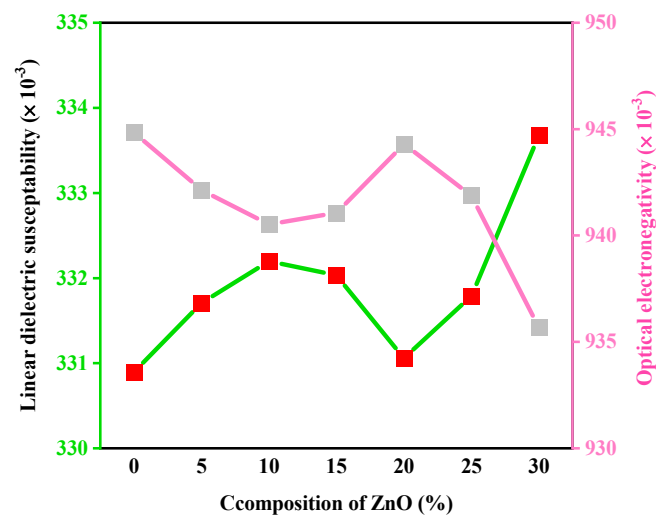


Figure 4. Variation in the linear dielectric susceptibility and optical electronegativity considering the amount of ZnO.

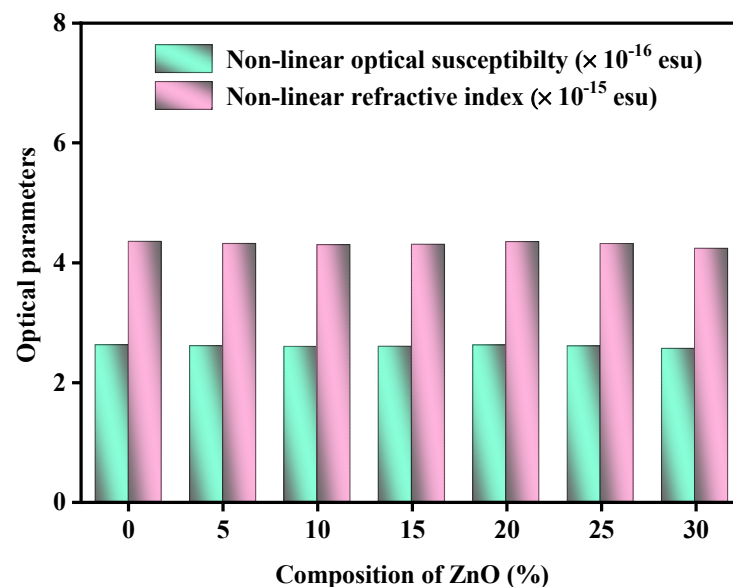


Figure 5. Variation in the non-linear optical susceptibility (χ^3) and non-linear refractive index considering the amount of ZnO.

The variation in reflection loss (RL) and transmission coefficient (T), considering the amount of ZnO on the studied glass systems, is displayed in Figure 2. The ZnO content in the glasses has a negligible effect on the RL and T. The RL reduces as the T grows little, and the other way around.

Figure 3 has displayed the variation in the molecular polarizability (α_m), the molecular refractivity (R_m), and the electronic polarizability (α_e), considering the amount of ZnO. When ZnO concentrations are increased, the values of the molecular polarizability (α_m) and the molecular refractivity (R_m) drop from 18.767 – 15.018 cm^3/mol and from 7.444×10^{-24} – 5.957×10^{-24} cm^3 , correspondingly; while the electronic polarizability (α_e) rises, from 8.244×10^{24} – 8.273×10^{24} , this is because the increased ZnO concentration for the glasses causes a rise in NBOs.

The values of metallization (M), energy band gap-based metallization ($M(E_g)$), and refractive index-based metallization ($M(n)$) are essentially constant at values of around 0.151, 0.088, and 0.418, respectively. Clearly, the produced glass structures are non-metallic in nature, since all values are less than one.

Variation in the linear dielectric susceptibility and optical electronegativity considering the amount of ZnO is demonstrated in Figure 4. Due to the increase in the quantity of NBOs with increasing ZnO concentration, the value of χ^* comes down through 0.945–0.936, even though $\chi^{(1)}$ amplified in the range of 0.331–0.334.

Figure 5 illustrates the variation in the non-linear optical susceptibility (χ^3) and non-linear refractive index, considering the amount of ZnO. Estimates of the present glass samples' non-linear optical susceptibility (χ^3) and non-linear refractive index (n_2^{optical}) decreased from 2.620×10^{-16} – 2.558×10^{-16} esu and from 4.348×10^{-15} – 4.230×10^{-15} esu, respectively. It is possible that the increased concentration of NBOs in the tested glasses is to blame.

3.2. Radiation Shielding Study

Figure 6 reveals the arrangements of linear attenuation coefficients (LAC) according to the incident photon energy of the studied glass samples between the 0.0395–0.344 MeV energy array. In this work, a very low energy of 0.0395–0.344 MeV was considered, which is the difference between the current work and the previous work by Effendy et al. [30]. Between the incident photon energy array of 0.0395–0.3443 MeV, these studied glass samples showed a sharp decrease in the LAC values having energy enhancement.

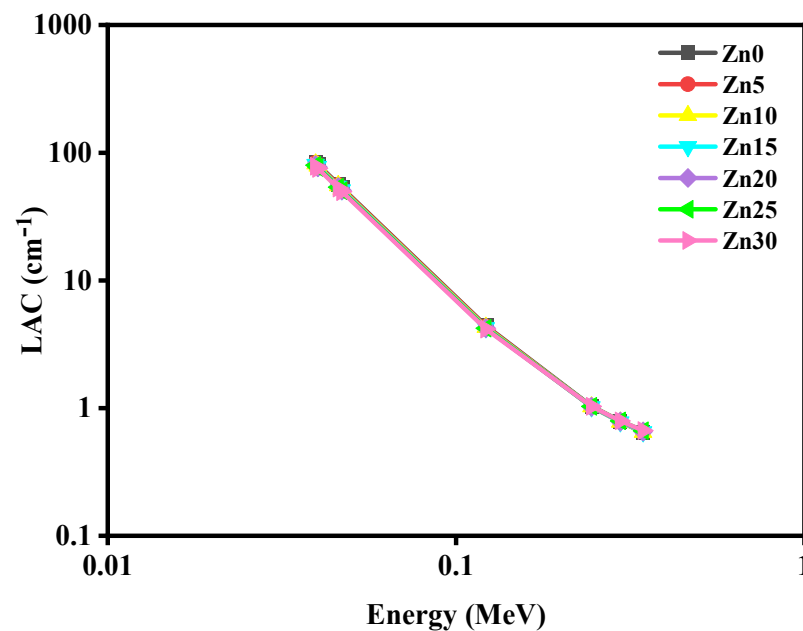


Figure 6. The performance of the linear attenuation coefficients (LAC) of the studied glass samples at studied energies.

Figure 7 demonstrates that the schemes of mass attenuation coefficients (MAC) of the studied glass samples counter the energy range 0.0395–0.3443 MeV. From this figure, it is clear that the evaluated MAC values of the studied glass samples decreased through increasing photon energy. Here, the values of MAC for the studied glass samples followed a very little decreasing trend $\text{Zn0} > \text{Zn5} > \text{Zn10} > \text{Zn15} > \text{Zn20} > \text{Zn25} > \text{Zn30}$ from energy range 0.0395–0.1218 MeV; however, there is a negligible variation obtained from the energy range of 0.2447–0.3443 MeV. The values of MAC presented a greater value at a studied lower energy range from 0.0395–0.047 MeV, yet, showed lesser values at a studied higher energy range from 0.1218–0.3443 MeV. Moreover, the MAC values displayed 1.6 times higher values through enhancing the energy range 0.0395–0.047 MeV; nevertheless, from an energy of 0.047–0.1218 MeV, the MAC values amplified by 8.4 times.

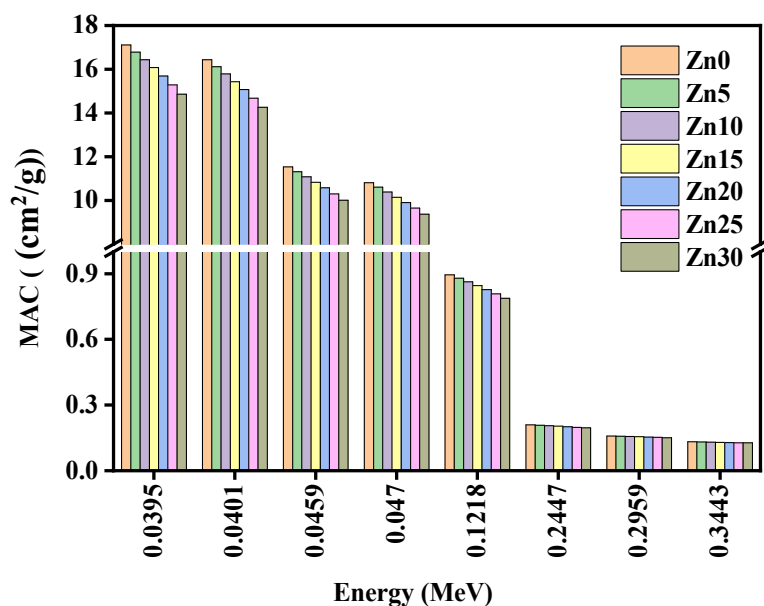


Figure 7. The performance of the mass attenuation coefficients (MAC) of the studied glass samples at studied energies.

The behavior of the half value layer (HVL) of the studied glass Zn30 sample is shown in Figure 8 against photon energy. This figure reveals an increasing value of half value layer through enhancing photon energy from 0.0395–0.3443 MeV. However, considering the studied glass sample, it was observed that the HVL for the studied sample of Zn30 was enhanced by 117 times higher values from an energy of 0.0395 MeV to 0.3443 MeV.

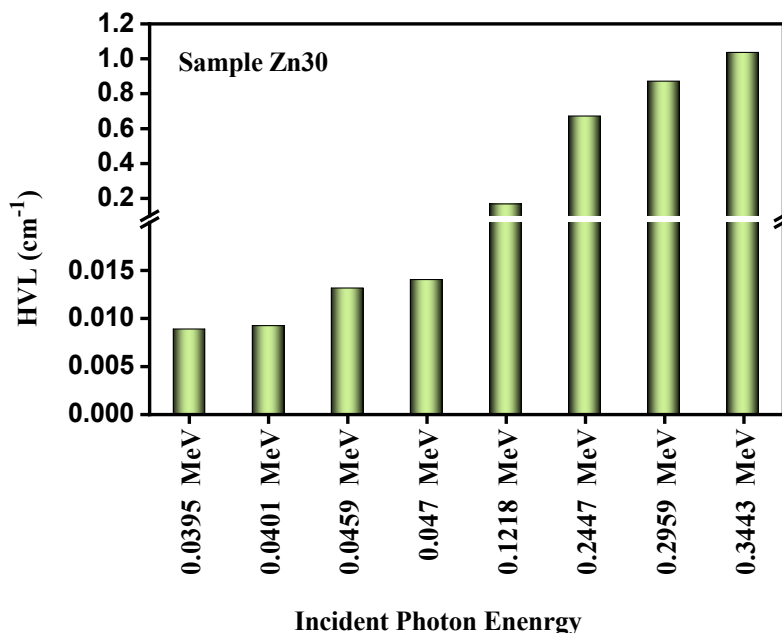


Figure 8. The performance of the HVL of the studied glass samples of Zn30 for the studied energies.

Figure 9 shows the value of the HVL of all studied glass samples at an energy of 0.3443 MeV. It is clear that the Zn10 sample displayed the greatest value of 1.068 cm and the Zn30 sample revealed the lowest value of 1.037 cm, which exemplifies that sample Zn30 has the compositional glass among the studied glass samples for radiation shielding.

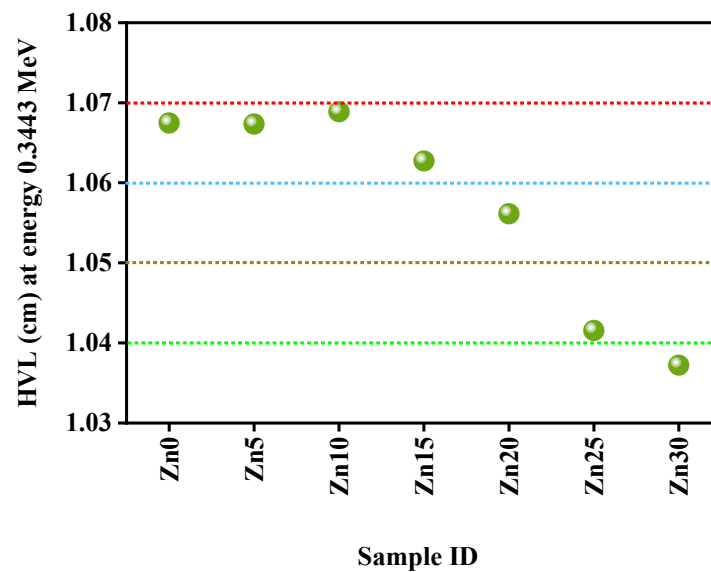


Figure 9. Presentation of the half value layer of all studied glass samples at an energy of 0.3443 MeV.

Figure 10 illustrates the MFP deeds of studied glass samples at the energy range 0.0395–0.3443 MeV. The MFP of the considered glass samples has displayed an increasing attitude through the intensification of incident photon energy.

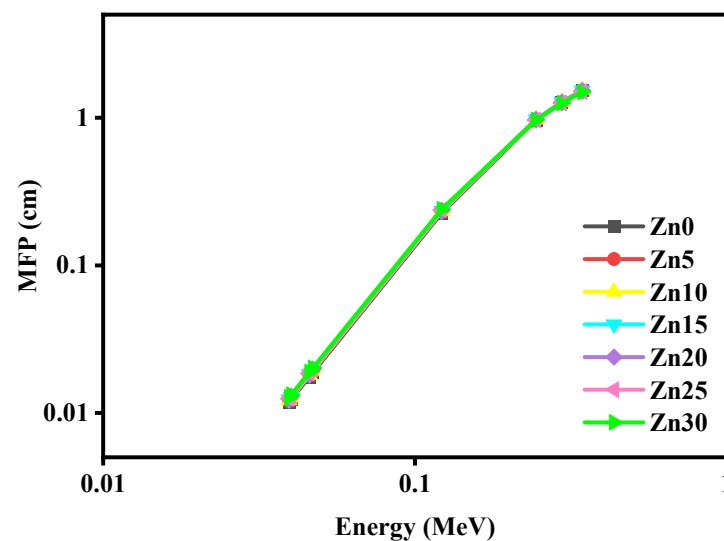


Figure 10. The performance of the MFP of the studied samples for the studied energies.

This suggests that a thin layer of Zn-X glasses is needed to shield the low-energy photons, while when the energy of the radiation is increased; we need a thicker glass to enhance the shielding performance of the glass. This is in line with the recent results for other glass systems [31–33]. Additionally, we found that the addition of ZnO has an impact on the MFP. Since the addition causes an increase in the density from 4.939 to 5.283 g/cm³, then the MFP slightly decreases and this is acceptable according to the inverse relation between the MFP and the density of the shield.

Figure 11 portrays the discrepancy of the Z_{eff} of the studied glass samples through the photon energy range 0.0395–0.3443 MeV. It has been obtained that the Z_{eff} of the studied glass samples has decreased through enhancing photon energy. Plainly, a sharp declination has been demonstrated for the values of Z_{eff} of the studied glass samples from the energy range 0.1218–0.3443 MeV.

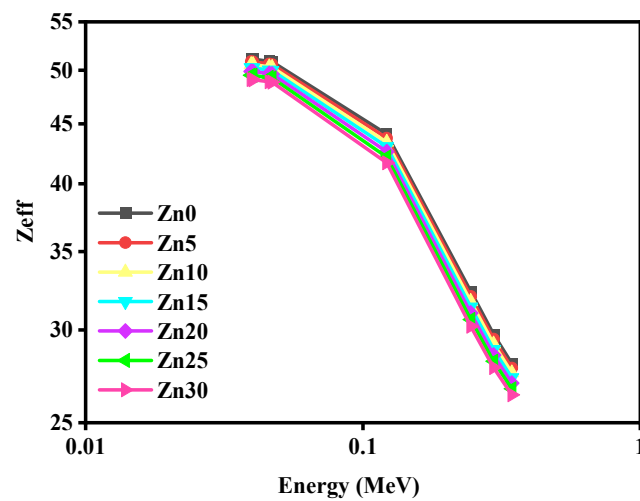


Figure 11. The performance of the effective atomic number of the studied glass samples for the studied energies.

The value of the Z_{eff} of all the considered samples has been demonstrated for an energy of 0.1218 MeV (Figure 12). Sample Zn30 showed the minimum value of Z_{eff} likening to other samples because of the lower amount of TeO_2 , conclusively, the studied glass Zn0 sample appeared to be the maximum value of Z_{eff} among the other studied samples.

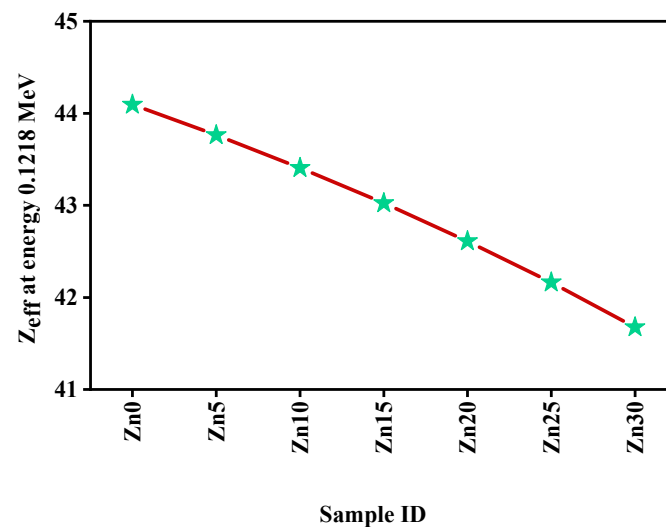


Figure 12. The performance of the Z_{eff} for all studied glass samples at energy 0.1218 MeV.

4. Conclusions

The radiation defensive efficiency and the optical features of the TeO_2 glass matrix were analyzed considering the effect of the concentration of the ZnO modifier. The introduction of ZnO into the TeO_2 network results in a decrease in the value of the indirect band gap, which goes from 3.515 to 3.481 eV. The values of the refractive index, dielectric constant, and optical dielectric constant all increased between the ranges 2.271–2.278, 5.156–5.191, as well as 4.156–4.191, accordingly. Transmission coefficient and reflection loss operate in a manner that is opposed to one another. With an increase in ZnO concentration in the selected glasses, the values of molar refractivity and molar polarizability decrease from $18.767 \text{ cm}^3/\text{mol}$ to $15.018 \text{ cm}^3/\text{mol}$ and from $7.444 \times 10^{-24} \text{ cm}^3$ to $5.957 \times 10^{-24} \text{ cm}^3$, respectively. On the other hand, the electronic polarizability increases from 8.244×10^{24} to 8.273×10^{24} . The metallization values support that the glass systems have a non-metallic fundamental composition. Regarding the values of LAC, MAC, HVL, MFP, and Z_{eff} , the Zn30 sample showed the best radiation shielding ability comprising other studied samples.

Author Contributions: Data curation, M.I.S.; Funding acquisition, D.A.A. and A.H.A.; Investigation, A.K.; Methodology, S.Y.; Project administration, A.H.A.; Supervision, D.A.A.; Writing—original draft, M.I.S. and S.Y.; Writing—review & editing, A.K. All authors have read and agreed to the published version of the manuscript.

Funding: This research was funded by Princess Nourah bint Abdulrahman University Researchers Supporting Project number (PNURSP2022R57), Princess Nourah bint Abdulrahman University, Riyadh, Saudi Arabia.

Institutional Review Board Statement: Not applicable.

Informed Consent Statement: Not applicable.

Data Availability Statement: Not applicable.

Acknowledgments: This research was funded by Princess Nourah bint Abdulrahman University Researchers Supporting Project number (PNURSP2022R57), Princess Nourah bint Abdulrahman University, Riyadh, Saudi Arabia.

Conflicts of Interest: The authors declare no conflict of interest.

References

1. Araz, A.; Kavaz, E.; Durak, R. Neutron and photon shielding competences of aluminum open-cell foams filled with different epoxy mixtures: An experimental study. *Radiat. Phys. Chem.* **2021**, *182*, 109382. [[CrossRef](#)]
2. Abouhaswa, A.S.; Kavaz, E. Bi₂O₃ effect on physical, optical, structural and radiation safety characteristics of B₂O₃-Na₂O-ZnO-CaO glass system. *J. Non-Cryst. Solids* **2020**, *535*, 119993. [[CrossRef](#)]
3. Dong, M.; Zhou, S.; Xue, X.; Feng, X.; Yang, H.; Sayyed, M.; Tishkevich, D.; Trukhanov, A.; Almousa, N. Upcycling of boron bearing blast furnace slag as highly cost-effective shield for protection of neutron radiation hazard: An innovative way and proposal of shielding mechanism. *J. Clean. Prod.* **2022**, *355*, 131817. [[CrossRef](#)]
4. Rajesh, M.; Kavaz, E. Deva Prasad Raju, Photoluminescence, radiative shielding properties of Sm³⁺ ions doped fluoroborosilicate glasses for visible (reddish-orange) display and radiation shielding applications. *Mater. Res. Bull.* **2021**, *142*, 111383. [[CrossRef](#)]
5. Gökçe, H.S.; Öztürk, B.C.; Çam, N.F.; Andiç-Çakır, Ö. Gamma-ray attenuation coefficients and transmission thickness of high consistency heavyweight concrete containing mineral admixture. *Cem. Concr. Compos.* **2018**, *92*, 56–69. [[CrossRef](#)]
6. Dong, M.; Zhou, S.; Xue, X.; Feng, X.; Sayyed, M.I.; Khandaker, M.U.; Bradley, D.A. The potential use of boron containing resources for protection against nuclear radiation. *Radiat. Phys. Chem.* **2021**, *188*, 109601. [[CrossRef](#)]
7. Dong, M.; Zhou, S.; Xue, X.; Sayyed, M.; Tishkevich, D.; Trukhanov, A.; Wang, C. Study of comprehensive shielding behaviors of chambersite deposit for neutron and gamma ray. *Prog. Nucl. Energy* **2022**, *146*, 104155. [[CrossRef](#)]
8. Dong, M.; Xue, X.; Yang, H.; Li, Z. Highly cost-effective shielding composite made from vanadium slag and boron-rich slag and its properties. *Radiat. Phys. Chem.* **2017**, *141*, 239–244. [[CrossRef](#)]
9. Tishkevich, D.I.; Grabchikov, S.S.; Lastovskii, S.B.; Trukhanov, S.V.; Vasin, D.S.; Zubar, T.I.; Kozlovskiy, A.L.; Zdorovets, M.V.; Sivakov, V.A.; Muradyan, T.R.; et al. Function composites materials for shielding applications: Correlation between phase separation and attenuation properties. *J. Alloys Compd.* **2019**, *771*, 238–245. [[CrossRef](#)]
10. Dong, M.; Xue, X.; Yang, H.; Liu, D.; Wang, C.; Li, Z. A novel comprehensive utilization of vanadium slag: As gamma ray shielding material. *J. Hazard. Mater.* **2016**, *318*, 751–757. [[CrossRef](#)] [[PubMed](#)]
11. Cheewasukhanont, W.; Limkitjaroenporn, P.; Kothan, S.; Kedkaew, C.; Kaewkhao, J. The effect of particle size on radiation shielding properties for bismuth borosilicate glass. *Radiat. Phys. Chem.* **2020**, *172*, 108791. [[CrossRef](#)]
12. Kamislioglu, M. An investigation into gamma radiation shielding parameters of the (Al:Si) and (Al+Na):Si-doped international simple glasses (ISG) used in nuclear waste management, deploying Phy-X/PSD and SRIM software. *J. Mater. Sci. Mater. Electron.* **2021**, *32*, 12690–12704. [[CrossRef](#)]
13. Sayyed, M.I.; Issa, S.A.M.; Tekin, H.O.; Saddeek, Y.B. Comparative study of gamma-ray shielding and elastic properties of BaO–Bi₂O₃–B₂O₃ and ZnO–Bi₂O₃–B₂O₃ glass systems. *Mater. Chem. Phys.* **2018**, *217*, 11–22. [[CrossRef](#)]
14. Sayyed, M.I.; Akyildirim, H.; Al-Buriah, M.S. Eloic Lacomme, Rachid Ayad, Giovanni Bonvicini, Oxyfluoro-tellurite-zinc glasses and the nuclear-shielding ability under the substitution of AlF₃ by ZnO. *Appl. Phys. A* **2020**, *126*, 88. [[CrossRef](#)]
15. Kamislioglu, M. Research on the effects of bismuth borate glass system on nuclear radiation shielding parameters. *Result Phys.* **2021**, *22*, 103844. [[CrossRef](#)]
16. Aktas, B.; Acikgoz, A.; Yilmaz, D.; Yalcin, S.; Dogru, K.; Yorulmaz, N. The role of TeO₂ insertion on the radiation shielding, structural and physical properties of borosilicate glasses, the role of TeO₂ insertion on the radiation shielding, structural and physical properties of borosilicate glasses. *J. Nucl. Mater.* **2022**, *563*, 153619. [[CrossRef](#)]
17. Ersundu, A.E.; Büyükyıldız, M.; Ersundu, M.Ç.; Şakar, E.; Kurudirek, M. The heavy metal oxide glasses within the WO₃-MoO₃-TeO₂ system to investigate the shielding properties of radiation applications. *Prog. Nucl. Energy* **2018**, *104*, 280–287. [[CrossRef](#)]

18. Aşkın, A. Gamma and neutron shielding characterizations of the $\text{Ag}_2\text{O}-\text{V}_2\text{O}_5-\text{MoO}_3-\text{TeO}_2$ quaternary tellurite glass system with the Geant4 simulation toolkit and Phy-X software. *Ceram. Int.* **2020**, *46*, 6040–6051. [[CrossRef](#)]
19. Sharma, A.; Nazrin, S.; Humaira, S.A.; Boukhris, I.; Kebaili, I. Impact of neodymium oxide on optical properties and X-ray shielding competence of $\text{Nd}_2\text{O}_3-\text{TeO}_2-\text{ZnO}$ glasses. *Radiat. Phys. Chem.* **2022**, *195*, 110047. [[CrossRef](#)]
20. Bektasoglua, M.; Ali Mohammad, M. Investigation of radiation shielding properties of $\text{TeO}_2-\text{ZnO}-\text{Nb}_2\text{O}_5-\text{Gd}_2\text{O}_3$ glasses at medical diagnostic energies. *Ceram. Int.* **2020**, *46*, 16217–16223. [[CrossRef](#)]
21. Nazrin, S.; Sharma, A.; Muhammad, S.; Alghamdi, N.A.; Wageh, S. Mechanical and radiation shielding properties of CuO doped $\text{TeO}_2-\text{B}_2\text{O}_3$ glass system. *Radiat. Phys. Chem.* **2022**, *198*, 110222. [[CrossRef](#)]
22. Fidan, M.; Acikgoz, A.; Demircan, G.; Yilmaz, D.; Aktas, B. Optical, structural, physical, and nuclear shielding properties, and albedo parameters of $\text{TeO}_2-\text{BaO}-\text{B}_2\text{O}_3-\text{PbO}-\text{V}_2\text{O}_5$ glasses. *J. Phys. Chem. Solids* **2022**, *163*, 110543. [[CrossRef](#)]
23. Geidam, I.G.; Matori, K.A.; Halimah, M.K.; Chan, K.T.; Muhammad, F.D.; Ishak, M.; Umar, S.A. Oxide ion polarizabilities and gamma radiation shielding features of $\text{TeO}_2-\text{B}_2\text{O}_3-\text{SiO}_2$ glasses containing Bi_2O_3 using Phy-X/PSD software. *Mater. Today Commun.* **2022**, *31*, 103472. [[CrossRef](#)]
24. Ersundu, M.Ç.; Ersundu, A.E.; Gedikoğlu, N.; Şakar, E.; Büyükyıldız, M.; Kurudirek, M. Physical, mechanical and gamma-ray shielding properties of highly transparent $\text{ZnO}-\text{MoO}_3-\text{TeO}_2$ glasses. *J. Non-Cryst. Solids* **2019**, *524*, 119648. [[CrossRef](#)]
25. Effendy, N.; Sidek, H.A.A.; Halimah, M.K.; Zaid, M.H.M. Enhancement on thermal, elastic and optical properties of new formulation tellurite glasses: Influence of ZnO as a glass modifier. *Mater. Chem. Phys.* **2021**, *273*, 125156. [[CrossRef](#)]
26. Şakar, E.; Özpolat, Ö.F.; Alım, B.; Sayyed, M.I.; Kurudirek, M. Phy-X/PSD: Development of a user friendly online software for calculation of parameters relevant to radiation shielding and dosimetry. *Radiat. Phys. Chem.* **2020**, *166*, 108496. [[CrossRef](#)]
27. Almuqrin, A.H.; Sayyed, M.; Kumar, A. Dielectric constant, polarizability, susceptibility and gamma ray shielding behavior of the $\text{Li}_2\text{O}-\text{Li}_2\text{MoO}_4-\text{TiO}_2-\text{P}_2\text{O}_5$ glasses. *Optik* **2021**, *245*, 167639. [[CrossRef](#)]
28. Alotaibi, B.M.; Sayyed, M.I.; Kumar, A.; Alotiby, M.; Sharma, A.; Al-Yousef, H.A.; Alsaif, N.A.; Al-Hadeethi, Y. Optical and gamma-ray shielding effectiveness of a newly fabricated $\text{P}_2\text{O}_5-\text{CaO}-\text{Na}_2\text{O}-\text{K}_2\text{O}-\text{PbO}$ glass system. *Prog. Nucl. Energy* **2021**, *138*, 103798. [[CrossRef](#)]
29. Agar, O.; Sayyed, M.; Tekin, H.; Kaky, K.M.; Baki, S.; Kityk, I. An investigation on shielding properties of BaO, MoO_3 and P_2O_5 based glasses using MCNPX code. *Results Phys.* **2019**, *12*, 629–634. [[CrossRef](#)]
30. Effendy, N.; Zaid, M.; Sidek, H.; Matori, K.; Mahmoud, K.; Sayyed, M. Influence of ZnO to the physical, elastic and gamma radiation shielding properties of the tellurite glass system using MCNP-5 simulation code. *Radiat. Phys. Chem.* **2021**, *188*, 109665. [[CrossRef](#)]
31. Alsaif, N.A.M.; Alotiby, M.; Hanfi, M.Y.; Sayyed, M.I.; Mahmoud, K.A.; Alotaibi, B.M.; Alyousef, H.A.; Al-Hadeethi, Y. A comprehensive study on the optical, mechanical, and radiation shielding properties of the $\text{TeO}_2-\text{Li}_2\text{O}-\text{GeO}_2$ glass system. *J. Mater. Sci. Mater. Electron.* **2021**, *32*, 15226–15241. [[CrossRef](#)]
32. Abouhaswa, A.S.; Kavaz, E. A novel $\text{B}_2\text{O}_3-\text{Na}_2\text{O}-\text{BaO}-\text{HgO}$ glass system: Synthesis, physical, optical and nuclear shielding features. *Ceram. Int.* **2020**, *46*, 16166–16177. [[CrossRef](#)]
33. Al-Yousef, H.A.; Alotiby, M.; Hanfi, M.Y.; Alotaibi, B.M.; Mahmoud, K.A.; Sayyed, M.I.; Al-Hadeethi, Y. Effect of the Fe_2O_3 addition on the elastic and gamma-ray shielding features of bismuth sodium-borate glass system. *J. Mater. Sci. Mater. Electron.* **2021**, *32*, 6942–6954. [[CrossRef](#)]